Voltage Interaction Evaluation in Embedded DC Transmission System

Cangbi Ding, Chenyi Zheng, Yi Tang, *Senior Member*, *IEEE*, Chaohai Zhang, and Xingning Han

***Abstract*—Voltage interaction between the rectifier and inverter buses is recognized as a critical factor in embedded direct current (EDC) transmission systems, where at least two ends are within a single synchronous AC network, as it significantly affects power flow distribution, voltage stability, and power system planning. Conventional methods for evaluating voltage interaction are insufficient to accurately represent the complicated interplay between responses of the AC-DC network and the internal controllers within EDC transmission systems. To address this issue, this paper proposes an analytical calculation method of a novel voltage interaction evaluation index for various types of EDC transmission systems, which enables precise evaluation of the voltage interaction between the rectifier bus and inverter bus in an EDC transmission system. The proposed method comprehensively accounts for the influence of voltage interaction under small disturbances through the AC network, as well as the influence of voltage interaction under the same disturbance between converter buses through internal controller responses. Numerical simulations are used to analyze the parametric dependence of the index, and its accuracy is demonstrated through dynamic simulation.**

***Index Terms*—DC transmission system, AC network, voltage interaction, parametric dependence.**

I. Introduction

HIGH-VOLTAGE direct current (HVDC) transmission systems, represented by line-commutated converter (LCC) HVDC, play a critical role in interconnecting regional grids and facilitating long-distance electric power transmission [1]-[3]. This transmission mode, where a DC link physically connects at least two ends within a single synchronous AC network, is defined as the embedded direct current (EDC) transmission system by CIGRE Joint Working Group C4/B4/C1.604, and it performs additional functions within the AC network such as power flow regulation, system stability improvement, and voltage control [4].

Voltage interaction among inverter buses of multiple EDC transmission systems exerts a profound influence on the system planning, design, and operation control [5] - [7]. The multi-infeed interaction factor (MIIF) is proposed by CIGRE to quantify the interaction degree between the inverter buses [8], [9], and the core concept of MIIF is to equate the critical short-circuit ratio (SCR) of a multi-infeed HVDC transmission system to that of a single-infeed HVDC transmission system based on the maximum power transfer theory of DC transmission systems [10], [11]. However, this factor is obtained from empirical simulation data, lacking the capability to reflect the structural and operational characteristics of the AC/DC grid from the perspective of mechanism analysis. Consequently, researches on analytical calculation methods for MIIF have been extensively studied, which can be divided into the following three categories. ① The mutual- and self-impedance values of the multiple inverter stations in the node impedance matrix are calculated in [12], [13] based on the multi-port equivalence principle to evaluate the inter-inverter interaction. ② An analytical expression is derived in [14], [15] for MIIF based on reasonable assumptions regarding the elements of the Jacobian matrix during the power flow equation calculation under small disturbances, effectively reflecting the dynamic characteristics of the network. ③ For hybrid multi-infeed HVDC transmission systems [16], a multi-infeed voltage interaction factor (MVIF) is proposed in [17] to quantify and evaluate the voltage interaction between different inverter station types, along with a corresponding analytical calculation method.

The aforementioned methods are effective in calculating the inter-inverter interaction in multiple regional EDC (R-EDC) transmission systems. However, with the development of provincial networks within the regional network, traditional expansion planning methods such as the construction of AC lines, can hardly satisfy the demands for increased transmission capacity, the suppression of short-circuit current, and integration of more renewable energy sources. Under this circumstance, the provincial EDC (P-EDC) transmission systems characterized by lower voltage level and shorter line length have started to emerge in actual provincial power grids [18], [19]. Different from R-EDC transmission sys-

Manuscript received: November 29, 2024; revised: April 14, 2025; accepted: June 27, 2025. Date of CrossCheck: June 27, 2025. Date of online publication: July 24, 2025.

This work was supported by the National Natural Science Foundation of China (No. 52377085). The author thanks State Grid Jiangsu Electric Power Company for providing valuable application scenarios of the embedded DC transmission system in the actual power grid, as well as the associated planning and design schemes.

C. Ding and C. Zhang are with College of Automation Engineering, Nanjing University of Aeronautics and Astronautics, Nanjing 211106, China (e-mail: dingcangbi26@126.com; zhangchaohai@nuaa.edu.cn).

C. Zheng is with College of Information Science and Technology and Artificial Intelligence, Nanjing Forestry University, Nanjing 210037, China (e-mail: zhengchenyi@njfu.edu.cn).

Y. Tang (corresponding author) is with School of Electrical Engineering, Southeast University, Nanjing 210096, China (e-mail: tangyi@seu.edu.cn).

X. Han is with Economic Research Institute, State Grid Jiangsu Electric Power Co., Ltd., Nanjing 210024, China (e-mail: xingning.han@qq.com).

DOI: 10.35833/MPCE.2024.001276

tems, such as the cross-provincial and high-capacity HVDC transmission system projects built in China, the European Union, Brazil, and other countries [1]-[22], the P-EDC transmission systems exhibit more significant interaction between the two ends [23], [24]. This interaction significantly affects key aspects such as the location of converter stations and the formulation of control strategies during the planning and operation of the EDC transmission systems, but only limited research has been conducted on analyzing the interaction between the rectifier bus and inverter bus in R-EDC transmission systems. An expression for the interaction factor in "inverter-rectifier multi-infeed" systems is derived in [25], [26] by constructing a Jacobian correction matrix that exclusively reflects the characteristics of the AC network, considering the influence of external control characteristics of different converter station types. Since voltage interaction in the P-EDC transmission system is further subject to the coupling influence of internal controllers between the rectifier station and inverter station, the existing methods cannot accurately quantify and analyze this characteristic, and it is difficult to distinguish between R-EDC transmission systems and P-EDC transmission systems from the perspective of interaction mechanism analysis.

To address the above issues, this paper presents a comparative analysis of different conventional methods used to calculate the voltage interaction between the converter buses in the EDC transmission system. Meanwhile, the analytical calculation method of a novel voltage interaction evaluation index for various types of EDC transmission systems is proposed, which combines the coupling influence of internal controller response on bus voltage under small disturbances with the conventional voltage interaction expression based on the Jacobian matrix. The electromagnetic transient simulation results based on a typical equivalent model of the EDC transmission system validate the effectiveness of the proposed method.

II. Discussion on Typical Structure of EDC Transmission Systems

The R-EDC and P-EDC transmission systems exhibit significant differences in their embedded structural configurations within the power grid, and the R-EDC transmission system is characterized by the interconnection of its rectifier station and inverter station through provincial networks under the regional network. The P-EDC transmission system consists of two converter stations located within the same provincial network, with a relatively short electrical distance between both ends, which mainly improves the transmission capacity of the provincial transmission section.

Various EDC transmission system projects in the synchronous AC grid are used as examples to illustrate the differences between different types of EDC transmission systems in interaction and operation characteristics, as shown in Fig. 1, where networks A and B denote the central and eastern China grids, respectively [4]. Figure 1(a) illustrates the Three Gorges−Changzhou DC project, which is an LCC-based R-EDC transmission system, with a DC line length of approximately 860 km [4], and the rectifier station and inverter station are located in Hubei Province and Jiangsu Province, respectively. Figure 1(b) illustrates the Cross Yangtze River DC project, which exemplifies an LCC-based P-EDC transmission system in Jiangsu Province, part of the eastern China grid, featuring a DC line length of approximately 200 km. Meanwhile, significant differences can be observed in the DC voltage levels U_d and DC transmission power capacities P_d of these two EDC transmission system projects.

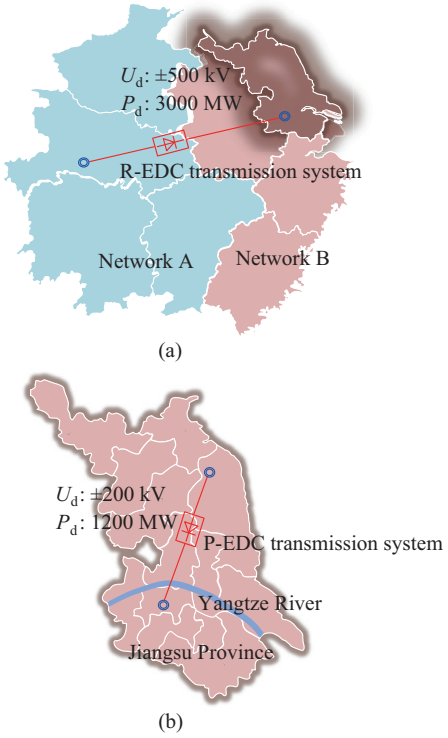

Fig. 1. EDC transmission system projects in actual power grid. (a) R-EDC transmission system project. (b) P-EDC transmission system project.

In the R-EDC transmission system, the substantial transmission distances typically result in disturbance occurring at one end having negligible influence on the AC network connected to the other end. Consequently, the existing researches disregard the interaction between the two ends of the EDC transmission system through the AC network. However, in the P-EDC transmission system, the electrical distance between the two ends of the EDC transmission system is substantially reduced. As a result, the disturbances that occur in the AC network at one end can directly influence the electrical quantities of the converter station and the corresponding AC network at the other end. In contrast to the decoupled operation characteristics of the R-EDC transmission system, the P-EDC transmission system exhibits stronger interaction between its ends.

It is evident that defining both types of DC transmission system projects in Fig. 1 as EDC transmission systems, as proposed by CIGRE, fails to accurately capture the significant differences in their interaction and operation characteristics. Due to the high voltage dependence of each converter station on the AC network, the definition of different types of EDC transmission systems can be further refined and enriched by quantifying the voltage interaction between the

two ends, thereby providing a more comprehensive depiction of the coupling influence.

III. Limitations in Voltage Interaction Analysis of EDC Transmission Systems

A. Voltage Interaction in EDC Transmission System

Sharing the same operation principle as the DC projects illustrated in Fig. 1, LCC-based EDC transmission system projects have been widely applied in actual power grids. Therefore, the LCC-based EDC transmission system is abstracted as a typical topology shown in Fig. 2 based on a two-port Thevenin equivalent principle, in which the rectifier bus and inverter bus are connected through the DC line and AC line. In Fig. 2, *VIFA* is the evaluation index of voltage interaction factor under the small disturbance between converter buses through the AC network in the EDC transmission system; *VIFC* is the evaluation index of voltage interaction factor under the small disturbance between converter buses through internal controller responses in the EDC transmission system; *EVIF* is the proposed evaluation index of the voltage interaction factor for various types of EDC transmission systems; Z_{sr} and Z_{si} are the equivalent impedances of AC network at both ends; P_r and Q_r are the active and reactive power outputs from the rectifier AC network, respectively; P_i and Q_i are the active and reactive power transmitted from the rectifier AC network to the inverter AC network through the external AC network and the EDC transmission system, respectively; P_{ri} and Q_{ri} are the active and reactive power transmitted through the external AC network, respectively; and P_d and Q_d are the active and reactive power transmitted through the EDC transmission system, respectively. It is important to note that, for the convenience of subsequent calculations and analysis, the external AC network between the two converter buses of the EDC transmission system is reduced and equivalently modeled as Z_{eq} [27]. Z_{eq} represents the electrical distance between the two ends of the EDC transmission system, and its magnitude is positively correlated with the electrical distance between the two converter buses.

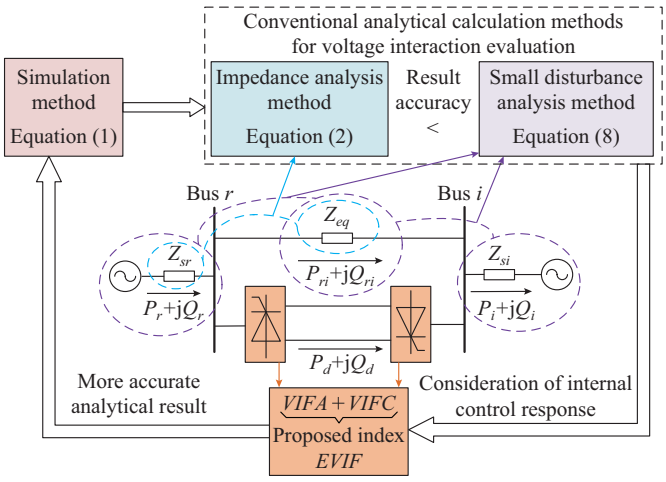

Fig. 2. Typical topology of LCC-based EDC transmission system and logical relationship between different voltage interaction evaluation methods.

In the evaluation methods of voltage interaction for DC transmission systems, $MIIF_{ji}$ is a main index used to evaluate the voltage interaction between inter-inverter buses through simulation, which is defined as the rate of voltage variation at the adjacent inverter bus j when the voltage at local inverter bus i drops by 0.01 p.u. [8]. Under most conditions, $MIIF_{ji} \in [0, 1]$, and $MIIF_{ji} = 0$ means that inverter stations of the two DC transmission systems are geographically or electrically isolated, resulting in negligible interaction. Conversely, $MIIF_{ji} = 1$ means that both DC transmission systems feed into the same inverter bus.

Analogous to the MIIF calculation method, which is widely recognized as a mature and well-established method for evaluating voltage interaction between converter buses, a similar simulation method can be applied to quantify the voltage interaction between the rectifier bus and inverter bus in the EDC transmission system as follows:

$$\frac{\Delta U_r}{\Delta U_i} = \frac{0.01\dfrac{\Delta U_r}{U_{r\mathrm{N}}}}{U_{drop}} \tag{1}$$

where ΔU_r is the voltage drop on the rectifier bus; ΔU_i is the voltage drop on the inverter bus; $U_{r\mathrm{N}}$ is the rated voltage of the rectifier bus; and U_{drop} denotes a voltage drop of 0.01 p.u. on the inverter bus.

The value of (1) is obtained by calculating the ratio between the voltage drop ΔU_r on the rectifier bus and ΔU_i (0.01 p.u.) that is caused by the inductive load connected to the inverter bus of the EDC transmission system on the simulation platform.

The value calculated from (1) indicates the interaction degree between the two ends of the EDC transmission system, and a higher value of (1) may exacerbate the propagation of system faults and expand the spatial impact of control strategy responses through the AC network.

B. Conventional Analytical Calculation Methods for Voltage Interaction

It is evident that the accurate value of voltage interaction defined in Section III-A is obtained through the electromagnetic transient simulation. However, this method requires detailed modeling of the target network, resulting in a high calculation cost and limiting its applicability in actual power grid analysis. Moreover, it performs poorly in both mechanism analysis and model scalability for voltage interaction. Therefore, the analytical calculation equation of voltage interaction, which is described in (1), needs to be established by referring to the analytical calculation method of the voltage interaction between converter buses, which is roughly divided into the impedance analysis method and small disturbance analysis method.

1) Impedance Analysis Method

This method is generally based on the bus impedance matrix of the typical topology of EDC transmission system in Fig. 2 to construct the analytical calculation equation of voltage interaction, which is recorded as the impedance ratio factor between converter buses in the EDC transmission system:

$$IRF = \frac{(\boldsymbol{Z})_{r,i}}{(\boldsymbol{Z})_{r,r}} \tag{2}$$

where $(\boldsymbol{Z})_{r,i}$ is the mutual impedance element between the converter buses in the bus impedance matrix $\boldsymbol{Z}$; and $(\boldsymbol{Z})_{r,r}$ is the self-impedance element of the rectifier bus in the bus impedance matrix $\boldsymbol{Z}$.

2) Small-disturbance Analysis Method Through AC Network

The core principle of this method is to determine the voltage interaction between buses based on the power distribution characteristics under small disturbances. In order to facilitate subsequent comparison and analysis and to obtain a relatively accurate analytical value of (1) without the influence of other factors, the inverter bus i shown in Fig. 2 is selected as the slack bus, with no power transmission in the AC line. The steady-state power flow equation of converter bus i in the EDC transmission system is expressed as:

$$\begin{cases} \Delta P_i = P_i - \left|U_i\right| \sum_{r=1}^{N} \left|U_r\right| (G_{ir}\cos(\delta_{ir}) + B_{ir}\sin(\delta_{ir})) + P_{di} \\ \Delta Q_i = Q_i - \left|U_i\right| \sum_{r=1}^{N} \left|U_r\right| (G_{ir}\sin(\delta_{ir}) - B_{ir}\cos(\delta_{ir})) + Q_{di} \end{cases} \tag{3}$$

where U_i and U_r are the voltages of bus i and bus r, respectively; N is the total number of adjacent buses to bus i; G_{ir} and B_{ir} are the conductance and susceptance between bus i and bus r, respectively; δ_{ir} is the phase difference between bus i and bus r; and P_{di} and Q_{di} are the active power and reactive power injected into bus i by the DC transmission system, respectively.

Since the transmission power of the DC transmission system is strongly coupled only with the voltage magnitude, its influence on the Jacobian matrix is reflected in the diagonal elements of block matrices $\boldsymbol{J}_{PU}$ and $\boldsymbol{J}_{QU}$. The following equation is the Jacobian matrix form of power flow calculation for networks with the EDC transmission system:

$$\begin{bmatrix} \Delta \boldsymbol{P} \\ \Delta \boldsymbol{Q} \end{bmatrix} = \begin{bmatrix} \boldsymbol{J}_{P\delta} & \boldsymbol{J}'_{PU} \\ \boldsymbol{J}_{Q\delta} & \boldsymbol{J}'_{QU} \end{bmatrix} \begin{bmatrix} \Delta \boldsymbol{\delta} \\ \Delta \boldsymbol{U}/\boldsymbol{U} \end{bmatrix} \tag{4}$$

where $\Delta\boldsymbol{P}$ and $\Delta\boldsymbol{Q}$ are the vectors of active and reactive power injection deviations at each bus, respectively; $\Delta\boldsymbol{\delta}$ is the vector of the bus voltage angle deviations; $\Delta\boldsymbol{U}/\boldsymbol{U}$ is the vector of the bus voltage magnitude deviations; and $\boldsymbol{J}_{P\delta}$, $\boldsymbol{J}_{Q\delta}$, $\boldsymbol{J}'_{PU}$, and $\boldsymbol{J}'_{QU}$ are the partial derivatives of the power flow equations of the converter bus with respect to the state variables. The diagonal elements $(\boldsymbol{J}'_{PU})_{i,i}$ and $(\boldsymbol{J}'_{QU})_{i,i}$ in $\boldsymbol{J}'_{PU}$ and $\boldsymbol{J}'_{QU}$ are modified as follows:

$$\begin{cases} (\boldsymbol{J}'_{PU})_{i,i} = (\boldsymbol{J}_{PU})_{i,i} - \dfrac{\partial (\boldsymbol{P}_{dc})_{i,i}}{\partial U_i} \\ (\boldsymbol{J}'_{QU})_{i,i} = (\boldsymbol{J}_{QU})_{i,i} - \dfrac{\partial (\boldsymbol{Q}_{dc})_{i,i}}{\partial U_i} \end{cases} \tag{5}$$

where $(\boldsymbol{J}_{PU})_{i,i}$ and $(\boldsymbol{J}_{QU})_{i,i}$ are the corresponding i^{th} diagonal elements of the inverter bus in the $\boldsymbol{J}_{PU}$ and $\boldsymbol{J}_{QU}$, respectively; and $\partial(\boldsymbol{P}_{dc})_{i,i}/\partial U_i$ and $\partial(\boldsymbol{Q}_{dc})_{i,i}/\partial U_i$ are the voltage sensitivities of bus i with respect to the active and reactive power injected by the converter station, respectively.

It is worth noting that, due to the various control strategies in the converter stations, the specific control strategy used by the DC transmission system connected to the converter buses needs to be considered when calculating the values of the diagonal elements $\partial P_{di}/\partial U_i$ and $\partial Q_{di}/\partial U_i$.

According to the physical definition for (1), only $\Delta\boldsymbol{Q}$ is considered in (4), i.e., $\Delta\boldsymbol{P} = \boldsymbol{0}$, and the relationship between $\Delta\boldsymbol{Q}$ and $\Delta\boldsymbol{U}/\boldsymbol{U}$ is:

$$\Delta \boldsymbol{Q} = \boldsymbol{J}_R \Delta \boldsymbol{U}/\boldsymbol{U} \tag{6}$$

$$\boldsymbol{J}_R = \boldsymbol{J}'_{QU} - \boldsymbol{J}_{Q\delta}\boldsymbol{J}_{P\delta}^{-1}\boldsymbol{J}'_{PU} \tag{7}$$

Finally, *VIFA* is described based on the elements of $\boldsymbol{J}_R$:

$$VIFA = \frac{\Delta U_{rac}/U_r}{\Delta U_i/U_i} = \frac{(\boldsymbol{J}_R^{-1})_{r,i}}{(\boldsymbol{J}_R^{-1})_{i,i}} \tag{8}$$

where ΔU_{rac} is the voltage drop of the rectifier bus under the influence of the AC network; $(\boldsymbol{J}_R^{-1})_{i,i}$ is the i^{th} diagonal element of $\boldsymbol{J}_R^{-1}$; and $(\boldsymbol{J}_R^{-1})_{r,i}$ is the r^{th} row and i^{th} column element of $\boldsymbol{J}_R^{-1}$.

C. Limitations of Existing Analytical Calculation Methods

Figure 2 illustrates the relationship between different voltage interaction evaluation methods. The influence of voltage fluctuation of the inverter bus on the rectifier bus is captured under the calculation process of actual value of (1). Given the strong coupling relationship between the bus voltage and the reactive power distribution along its branches, the focus of voltage interaction between converter buses needs to account for the trend of reactive power distribution on the target bus. However, *IRF* only demonstrates the structural characteristics and cannot reflect the characteristics of the reactive power distribution. *VIFA*, derived from the solving process of the power flow equation, considers not only the parameters of the network structure but also the influence of output characteristics of controllers such as converter stations of DC transmission systems. This is specifically represented in (7), where the elements of $\boldsymbol{J}_R$ incorporate the partial derivatives relating to the power exchange in the converter stations and the resulting voltage fluctuations. Therefore, the calculation result accuracy of *VIFA* is superior to that of *IRF*.

However, due to the strong interaction exhibited by the P-EDC transmission system between the two ends in a synchronous AC network, voltage interaction under these conditions must account for both the internal and external influences of converter stations. This coupling characteristic is ignored when calculating *VIFA*, as *VIFA* only considers the external control characteristics of converter stations. To achieve more accurate analytical results for voltage interaction, it is necessary to quantify the interaction between the two ends under the response of the internal controllers of converter stations, in addition to the existing *VIFA*. Through the comprehensive consideration of these two indices, a more precise characterization of the voltage interaction between both ends of the EDC transmission system can be obtained.

IV. Voltage Interaction Factor in EDC Transmission System

A. Steady-state Operation Principle of DC Transmission System

This paper takes the unipolar LCC-HVDC transmission

system operating under the rated condition as an example, and the expression for the DC current $I_{d\mathrm{N}}$ on the DC line is as follows:

$$I_{d\mathrm{N}} = \frac{U_{di} - U_{dr}}{R_d} \tag{9}$$

$$\begin{cases} U_{di} = U_{di0}\cos(\gamma) - X_{di} I_d \\ U_{dr} = U_{dr0}\cos(\alpha) - X_{dr} I_d \end{cases} \tag{10}$$

where U_{dr} and U_{di} are the DC voltages of rectifier station and inverter station, respectively; U_{dr0} and U_{di0} are the ideal no-load DC voltages of the rectifier station and inverter station, respectively; X_{dr} and X_{di} are the equivalent commutation reactances of the rectifier station and inverter station, respectively; γ is the inverter extinction angle; I_d is the DC current; α is the rectifier delay angle; and R_d is the equivalent resistance of the DC line.

The converter stations at both ends of the LCC-HVDC transmission system are equipped with controllers such as constant current (CC) controller, constant extinction angle (CEA) controller, current error controller (CEC), voltage dependent direct current order limiter (VDCOL) controller, and maximum delay angle controller, which keep the electrical quantities of the DC transmission system close to the rated operation condition and provide active adjustment capability during the transient process.

The typical control diagram of LCC-HVDC transmission system is shown in Fig. 3, where G is the gain factor; T is the time constant; I_{des} is the limited value of the output order of the VDCOL controller; I_{dref} is the output order of the VDCOL controller; I_{dref0} is the real-time output order of the VDCOL controller; β_γ and β_i are the output orders of the CEA controller and CC controller, respectively; β is the advance firing angle; γ_{des} is the limited value of the input order of the CEA controller; γ_{N} is the reference value of the CEA controller; and PI stands for proportional-integral. During steady-state operation, the rectifier station and inverter station generally adopt the CC controller and CEA controller, respectively, which is realized by adjusting the trigger angle to track set reference values I_{dref} and γ_{ref}.

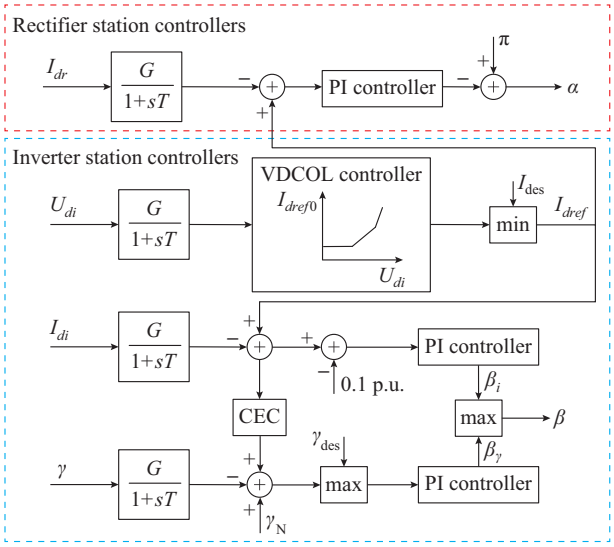

Fig. 3. Typical control diagram of LCC-HVDC transmission system.

Take the rectifier station as the research object to analyze the relationship between the active power transmission P_{dc} of the DC transmission system and the reactive power demand Q_{dc} of the rectifier station, and the mathematical expression is as follows:

$$\begin{cases} P_{dc} = U_{dr} I_d \\ Q_{dc} = Q_{acr} + Q_F \\ Q_{dc} = P_{dc}\tan(\varphi_r) \\ \varphi_r = \arccos(U_{dr}/U_{dr0}) \end{cases} \tag{11}$$

where φ_r is the power factor angle of the rectifier station; Q_{acr} is the reactive power exchanged between the DC transmission system and the AC network; and Q_F is the reactive power provided by the reactive power compensation devices configured in the rectifier station.

According to the expression of (11), the rectifier station can be regarded as an inductive load during steady-state operation, and Q_{dc} is mainly determined by φ_r and P_{dc}, which is generally supported by Q_F and Q_{acr}.

B. Analytical Calculation of Voltage Interaction Under Internal Controller Response

During the response of the CC controller, the DC current I_d' in the disturbance is consistent with $I_{d\mathrm{N}}$, i.e., $I_{d\mathrm{N}} = I_d'$. Combining with (9) and (10), if the voltage of the inverter bus drops by ΔU_i, the relationship between I_d before and after the disturbance is described as:

$$\frac{U_{di0}\cos(\gamma_{ref}) - X_{di} I_{d\mathrm{N}} - (U_{dr0}\cos(\alpha) - X_{dr} I_{d\mathrm{N}})}{R_d} = \frac{(U_{di0} - \Delta U_i)\cos(\gamma') - X_{di} I_d' - (U_{dr0}\cos(\alpha') - X_{dr} I_d')}{R_d} \tag{12}$$

Meanwhile, the CEA controller is adopted in the inverter station, i.e., $\gamma' = \gamma_{ref}$ and all other electrical quantities in (12) remain constant. Only α is adjusted to ensure the validity of (12), so the expression for α' during the small disturbance is:

$$\alpha' = \arccos\frac{U_{dr0}\cos(\alpha) - \Delta U_i \cos(\gamma_{\mathrm{N}})}{U_{dr0}} \tag{13}$$

Variation of α directly affects U_{dr} and φ_r, thus, the active power transmission of the DC transmission system and the reactive power demand of the rectifier station are changed, respectively:

$$\begin{cases} P_{dc}' = U_{dr}' I_d' \\ Q_{dc}' = P_{dc}\tan(\varphi_r') \\ \varphi_r' = \arccos(U_{dr}'/U_{dr0}) \\ U_{dr}' = U_{dr0}\cos(\alpha') - X_{dr} I_{d\mathrm{N}} \end{cases} \tag{14}$$

where φ_r' and U_{dr}' are the power factor angle and the DC voltage of the rectifier station under disturbance, respectively; and Q_{dc}' and P_{dc}' are the real-time active and reactive power exchange values of the rectifier station under the small disturbance, respectively, and can be directly used for the analytical calculation of *EVIF*.

The electromagnetic transient simulation is conducted in the CIGRE benchmark model to analyze the characteristics of different electrical quantities under the small disturbance

to prove the rationality of the above derivation. When an inductive load connected to the inverter bus results in a voltage drop of $\Delta U_i = 0.01$ p.u., the operation curves of I_d, γ, and α under the small disturbance are shown in Fig. 4. As a result of the influence of CC controller and CEA controller, the operation curves of I_d and γ exhibit negligible variation, and the operation curve of α experiences significant fluctuations.

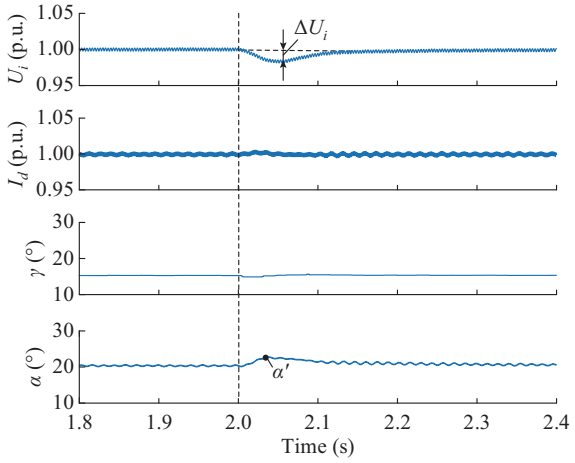

Fig. 4. Operation curves of I_d, γ, and α under small disturbance.

To evaluate the voltage interaction between the two ends of the DC transmission system without considering the influence of the AC network, the topology shown in Fig. 2, which does not include external AC network, is used as the research object. The similar calculation method as in (1) is adopted, and *VIFC* is obtained through simulation, which can be expressed as:

$$VIFC = \frac{|\Delta U_r|}{\Delta U_i} = \frac{|\tilde{U}_r - \tilde{U}_r'|}{\Delta U_i} \tag{15}$$

where $\tilde{U}_r$ is the phase value of the rectifier bus voltage under rated operation; and $\tilde{U}_r'$ is the phase value of the rectifier bus voltage under the small disturbance.

To facilitate the analysis of the variation of the rectifier bus under the small disturbance on the inverter bus, the rectifier AC network on the rectifier bus is equivalent to an open-ended network, containing a power source bus and a net load bus, as shown in Fig. 5. In Fig. 5, $\tilde{U}_{sr}$ is the phasor of the power source bus voltage; and P_{dc} is the active power on the net load bus.

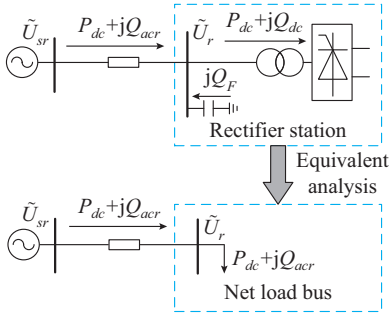

Fig. 5. Equivalent open-ended network on rectifier bus.

Under steady-state conditions, voltage drop exists between the power source bus and the net load bus in Fig. 5. The voltage relationship among buses in the equivalent open-ended network is illustrated in Fig. 6, and is expressed as:

$$\tilde{U}_r = \tilde{U}_{sr} - (\Delta U_{rdc} + j\delta U_{rdc}) \tag{16}$$

$$\begin{cases} \Delta U_{rdc} = \dfrac{P_{dc}R_{eqr} + Q_{acr}X_{eqr}}{U_r} \\ \delta U_{rdc} = \dfrac{P_{dc}X_{eqr} - Q_{acr}R_{eqr}}{U_r} \end{cases} \tag{17}$$

where R_{eqr} and X_{eqr} are the equivalent resistance and reactance of the rectifier AC network, respectively; and ΔU_{rdc} and δU_{rdc} are the vertical and horizontal components of the voltage drop value $d\tilde{U}_{rdc}$, respectively.

In Fig. 6, $\Delta U_{rdc}'$ and $\delta U_{rdc}'$ are the vertical and horizontal components of the voltage drop value $d\tilde{U}_{rdc}'$ under the small disturbance, respectively; and δ_0 and δ' are the phase differences under the rated operation and the small disturbance, respectively.

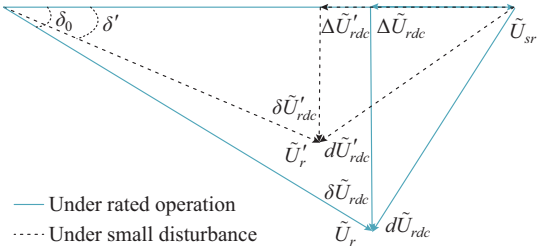

Fig. 6. Voltage relationship among buses in equivalent open-ended network.

Based on the above analysis, under the small disturbance on the inverter bus, P_{dc} and Q_{acr} on the net load bus are changed in Fig. 5. According to the voltage drop equation in the steady-state analysis of the power grid, and incorporating (15) to (17), $\tilde{U}_r'$ can be obtained.

$$\tilde{U}_r' = \tilde{U}_{sr} - (\Delta U_{rdc}' + j\delta U_{rdc}') \tag{18}$$

$$\begin{cases} \Delta U_{rdc}' = \dfrac{P_{dc}'R_{eqr} + Q_{acr}'X_{eqr}}{U_r} \\ \delta U_{rdc}' = \dfrac{P_{dc}'X_{eqr} - Q_{acr}'R_{eqr}}{U_r} \end{cases} \tag{19}$$

where P_{dc}' and Q_{acr}' are the active power and the reactive power on the net load bus under small disturbance, respectively.

Substituting $\tilde{U}_{rdc}'$ obtained from (18) into (15), *VIFC* is calculated to quantify the voltage interaction under the coupling influence of the internal controller response of the EDC transmission system.

C. Analytical Calculation Method of EVIF

The analytical calculation method of *VIFC* addresses the limitations of the *IRF* and *VIFA*, and the value of (1) is influenced by the values of the *VIFC* and *VIFA*. *EVIF* is proposed to clarify the mathematical implications of the voltage interaction, and its analytical calculation equation is ex-

pressed as:

$$EVIF = \begin{cases} VIFA & VIFA \geq VIFC \\ VIFC & VIFA < VIFC \end{cases} \tag{20}$$

The fundamental method for the analytical calculation of *EVIF* involves calculating both *VIFC* and *VIFA* under typical operation conditions based on (9) and (18), and the larger of the two values is chosen as the *EVIF* for the target EDC transmission system.

In (20), if $EVIF = VIFA$, it indicates the voltage drop on the inverter bus of the EDC transmission system has a more significant influence on the rectifier bus through the AC line than the influence of the internal control adjustments of the DC transmission system on the voltage fluctuation of the rectifier bus, and this kind of EDC transmission system can be classified as a P-EDC transmission system. Under the condition of $EVIF = VIFC$, the adjustment influence of the internal control system of the DC transmission system dominates the voltage influence of the inverter bus on the rectifier bus in the EDC transmission system. In this case, the AC connection between the inverter bus and rectifier bus is relatively weak, which can be regarded as an R-EDC transmission system. If $VIFA = VIFC$, *EVIF* is in a critical state, where the influence of the internal control system of the DC transmission system and the AC line both have the same voltage interaction between the rectifier bus and inverter bus of the EDC transmission system.

Different from $MIIF_{ji} \in [0, 1]$, the analytical calculation result of *EVIF* is never zero. This is because the defined analytical calculation equation of *EVIF* effectively captures the influence of both AC network operation characteristics and internal control response characteristics of the DC transmission system on the interaction of the EDC transmission system. Since *VIFA* and *VIFC* fully reflect the voltage interaction degree of the EDC transmission system, *EVIF* can be calculated using (20) under various conditions such as different target network, electrical distance, and SCR of AC networks, and this method enables a clearer delineation of the operational scope for the EDC transmission system and provides a theoretical basis for analyzing parameters that influence voltage interaction in the EDC transmission system.

V. Parametric Dependence of *EVIF*

A. Description of Simulation Model

The proposed method is utilized to systematically analyze, on the numerical analysis simulation platform, the parametric dependence of *EVIF* on the characteristics of the AC network in which the EDC transmission system operates. A typical simulation model of the EDC transmission system, as shown in Fig. 7, is constructed based on the CIGRE benchmark model, where the rectifier bus and inverter bus are interconnected via AC lines. In Fig. 7, U_{sr}, U_{si} and θ_{sr}, θ_{si} are the voltage magnitudes and phase angles of the power source buses at the rectifier and inverter AC networks, respectively; θ_r and θ_i are the voltage phase angles of the rectifier and inverter buses, respectively; z_{sr}, z_{si} and θ_{zsr}, θ_{zsi} are the magnitudes and phase angles of equivalent impedances of the rectifier and inverter AC networks, respectively; b_{cr} and b_{si} are the equivalent admittances of the reactive power compensation devices configured in the rectifier station and inverter station, respectively; z_{eq} and θ_{eq} are the magnitudes and phase angles of equivalent impedance of the external AC network, respectively; and φ_i is the power factor angle of the inverter station. Under the base condition, the SCRs of AC networks at both ends of the EDC transmission system are 2.5, and the base voltage and power of this typical simulation model are 345 kV and 1000 MW, respectively. The system parameter values are listed in Table I.

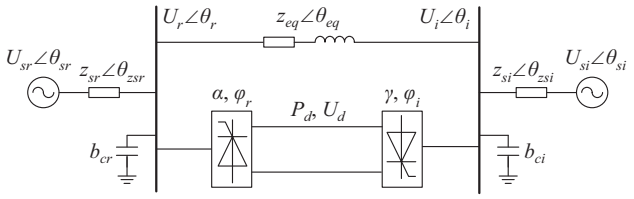

Fig. 7. Typical simulation model of EDC transmission system.

To ensure the accuracy of subsequent studies regarding the dependence of *EVIF* on different parameters, only the target parameter value in the simulation model is changed, while all other parameters remain constant. It should be noted that the following analysis focuses on the influence of AC network parameters on *EVIF* from the perspective of the overall operational capability of the system without considering the internal parameters of the EDC transmission system.

TABLE I
System Parameter Values Under Basic Condition

Unit	Parameter	Value
Rectifier AC network	$U_r\angle\theta_r$	$1.19\angle 19°$
	$z_{sr}\angle\theta_{zsr}$	$0.4\angle 84°$
	$U_{sr}\angle\theta_{sr}$	$1\angle 0°$
	b_{cr}	0.37
	α	32°
Transmission system	$z_{eq}\angle\theta_{eq}$	$0.34\angle 80°$
	P_d	0.6 p.u.
	U_d	±200 kV
	φ_r	35°
	φ_i	27°
Inverter AC network	$E_i\angle\theta_i$	$1.007\angle -22°$
	$z_{si}\angle\theta_{zsi}$	$0.4\angle 84°$
	$U_{si}\angle\theta_{si}$	$1\angle 0°$
	b_{ci}	0.37
	γ	15.9°

B. Dependence of VIFC

The accuracy of *VIFC* is the most important prerequisite for analytical calculation results of *EVIF* and its dependence parameters. Based on the proposed method in Section IV, the analytical calculation process for *VIFC* is illustrated using an example where SCR of the rectifier AC network (SCR_r) is set to be 2.5.

The inductive load connected to the inverter bus makes $\Delta U_i = 0.01$ p.u., and the parameter values related to *EVIF* under this disturbance is presented in Table II. Q'_{dc} and P'_{dc}, obtained from the analytical calculation under small disturbance, are substituted into (18) and (19), resulting in $U_r' = 0.99648$. According to the definition of *VIFC*, $VIFC = 0.352$ under $SCR_r = 2.5$.

TABLE II
PARAMETER VALUES RELATED TO *EVIF* UNDER DISTURBANCE OF $\Delta U_i = 0.01$ P.U.

ΔU_i (p.u.)	$\Delta\alpha$ (°)	$\Delta\varphi_r$ (°)	ΔQ_{dc} (p.u.)	ΔP_{dc} (p.u.)	ΔU_{rdc} (p.u.)
–0.01	0.25	0.808	0.024	–0.022	–0.00352

VIFC of the EDC transmission system under different SCR_r ($SCR_r \geq 2.5$) can be calculated by the above analytical calculation process. To ensure that the corresponding U_r remains at the rated value under different SCR_r, it is essential to dynamically adjust the grid-connected voltage value E_r of the equivalent power source on the rectifier AC network under each SCR_r. This adjustment can be achieved by employing optimization algorithms that identify the optimal E_r based on existing parameters such as Z_{sr} and U_r among other relevant parameter values. The results of *VIFC* with $SCR_r \in [2.5, 5.5]$ are calculated, and the relationship between SCR_r and *VIFC* presents a nearly proportional linear decreasing trend, as shown in Fig. 8. Under the same small disturbance, as the strength of the rectifier AC network gradually increases, ΔU_{rdc} progressively decreases, leading to a corresponding reduction in *VIFC*.

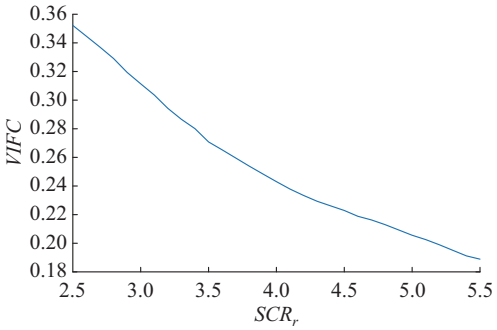

Fig. 8. Relationship between SCR_r and *VIFC*.

C. Dependence of Z_{eq}

The electrical distance of the external AC network of the EDC transmission system is directly characterized by adjusting the impedance value Z_{eq} as depicted in Fig. 2. Figure 9 illustrates the relationship between Z_{eq} and *EVIF* for the EDC transmission system under various SCR_r ($SCR_r = 2.5$, 3.5, 4.5, 5.5). Analysis of the respective curves indicates that, under any SCR_r, the trend of *EVIF* influenced by Z_{eq} remains fully consistent. When Z_{eq} approaches 0, *EVIF* asymptotically approaches 1, while when Z_{eq} approaches ∞, *EVIF* converges to its minimum value. This evidently indicates the broad applicability of *EVIF*, as it can be reliably derived under any electrical distance.

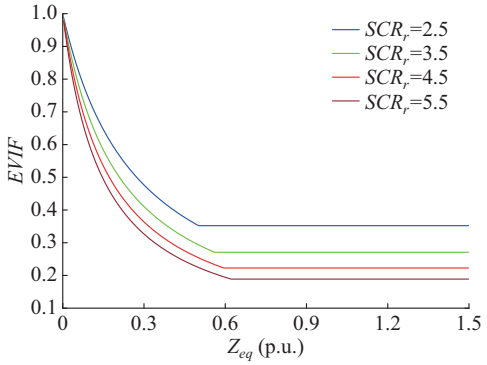

Fig. 9. Relationship between *EVIF* and Z_{eq}.

In the evaluation of *MIIF*, it is considered that when $MIIF > 0.6$, there is a strong coupling relationship between the two inverter buses. The evaluation of this index is analogous to *EVIF*. When $Z_{eq} < 0.14$ p.u., there is a strong interaction between the rectifier bus and inverter bus of the EDC transmission system, i. e., $EVIF > 0.6$. As Z_{eq} increases, *EVIF* decreases until it becomes constant, i. e., $EVIF = VIFC$, indicating that Z_{eq} is too long to affect the voltage interaction between the two converter buses of the EDC transmission system, and this type of EDC transmission system under this condition is considered as the R-EDC transmission system.

The absolute slope value k of *EVIF* for Z_{eq} directly reflects the influence degree of Z_{eq} on *EVIF*, and the relationship between k and Z_{eq} is shown in Fig. 10. The smaller the value of Z_{eq}, the more significant the influence of Z_{eq} on *EVIF*. Specifically, when $Z_{eq} < 0.19$ p. u., the value of k is high under any SCR_r, indicating that Z_{eq} within this range is the dominant dependence parameter for *EVIF*.

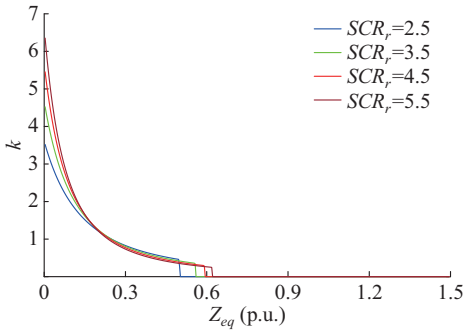

Fig. 10. Relationship between k and Z_{eq}.

D. Dependence of SCR_r

SCR is obtained by calculating the ratio between the short-circuit capacity of the external AC network and P_d of the EDC transmission system, and this parameter authoritatively reflects the interaction degree between the AC network and EDC transmission system. The relationship between *EVIF* and $SCR_r \in [2.5, 5.5]$ is shown in Fig. 11 under various Z_{eq} ($Z_{eq} = 0.30, 0.40, 0.50, 0.55, 0.60, 0.62$ p.u.).

When the rectifier AC network has the weakest support capability, i. e., $SCR_r = 2.5$, the critical Z_{eq} corresponding to *EVIF* is 0.50 p.u.. Hence, for $Z_{eq} \in (0, 0.50]$p.u., *EVIF* shows a linear relationship with SCR_r. In this range, if Z_{eq} is fixed,

EVIF decreases as SCR_r increases, and the reason is that an increase in SCR_r strengthens the support capability of the AC network for the rectifier bus, thus reducing the magnitude of ΔU_r caused by the same magnitude of ΔU_i.

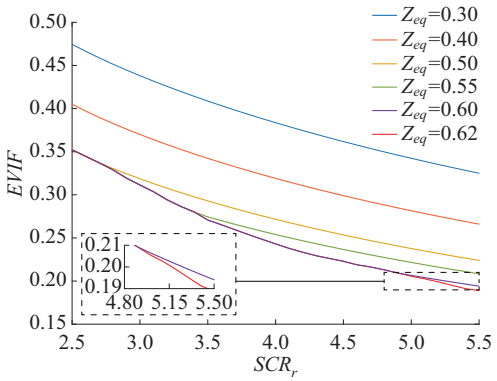

Fig. 11. Relationship between *EVIF* and SCR_r under various Z_{eq}.

As Z_{eq} further increases, the *EVIF* of the EDC transmission system for a certain range of SCR_r begins to converge, i. e., *EVIF* = *VIFC*. In Fig. 11, the overlapping part of the curves corresponding to $Z_{eq} = 0.50, 0.55, 0.60, 0.62$ p. u. indicates the convergence interval. For $Z_{eq} = 0.50, 0.55, 0.60$ p. u., the *EVIF* has converged within the ranges of $SCR_r \in [2.5, 2.7]$, $SCR_r \in [2.5, 3.4]$, $SCR_r \in [2.5, 4.9]$, respectively. Until $SCR_r = 5.5$, the corresponding critical Z_{eq} is 0.62 p.u., where all the observed *EVIF* converges within the SCR_r range. For an AC line with equal distance, the range of SCR_r for which *EVIF* converges gradually increases.

Since the SCR is determined by both the P_d and the short-circuit capacity, under the condition of a fixed short-circuit capacity in the AC network, the previously discussed relationship between SCR_r and *EVIF* can also reflect the correlation between P_d and *EVIF*.

Based on the analysis presented in Sections V-A, V-B, and V-C, the key parameters that significantly influence the analytical calculation results of *EVIF* include *VIFC*, Z_{eq}, and SCR_r. The relationship among *EVIF*, Z_{eq}, and SCR_r is illustrated in Fig. 12 ($SCR_r \in [2.5, 5.5]$, $Z_{eq} \in (0, 1.5]$p.u.).

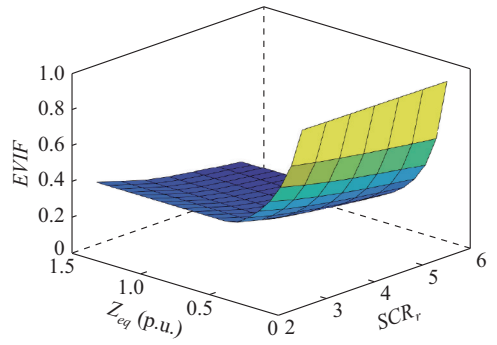

Fig. 12. Relationship among *EVIF*, Z_{eq}, and SCR_r.

From the perspective of comprehensive analysis, *VIFC* is a key index for distinguishing between different types of EDC transmission systems, directly influencing the distribution trend of *EVIF*. The values of Z_{eq} and SCR_r are instrumental in determining the analytical calculation result of *EVIF*, and the combined influence of these three parameters accurately reflects the interaction degree between the two ends of different types of EDC transmission systems.

VI. Comparison and Demonstration of Dynamic Simulation

A. Dynamic Simulation Model

Since conducting experiments in an actual power grid to obtain the value of (1) is impractical, establishing a full electromagnetic transient simulation model of the target network is a feasible method for accurately representing the real operation conditions of the power grid.

Therefore, to validate the accuracy of the proposed method for *EVIF* in Section IV-C, as well as to compare the analytical results of *IRF*, *VIFA*, and *EVIF*, a typical EDC transmission system model with basic condition completely consistent with those in Section V-A is constructed on the electromagnetic transient simulation platform PSCAD/EMTDC.

According to the definition in (1), during the dynamic simulation process, an inductive load is connected to the inverter bus at time t_0, causing $\Delta U_i = 0.01$ p.u.. The ΔU_r of the rectifier bus is then recorded, and $\Delta U_r / \Delta U_i$ is considered as the actual value of (1), which is used for error analysis below.

B. Analysis of Dynamic Simulation Results

The actual values of voltage interaction (1) under different Z_{eq} is shown as the red curve in Fig. 13 (the first recording point is at $Z_{eq} = 0.001$ p.u., the second at $Z_{eq} = 0.05$ p.u., with subsequent recording points with intervals of 0.05 p. u.). Combined with the parameter dependence analysis of *EVIF*, the dynamic simulation result curve presented in Fig. 13 can be divided into three phases.

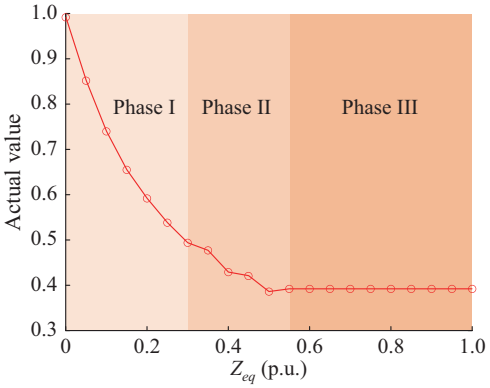

Fig. 13. Actual values of voltage interaction.

Phase I ($Z_{eq} \in (0, 0.30]$p.u.): as Z_{eq} increases, the curve of actual value of (1) has a clear and smooth downward trend, with the slope increasing from −2.79 to −0.88. Actual values are all higher than 0.48, indicating strong voltage interaction between the rectifier bus and inverter bus of the EDC transmission system during this phase. Combined with (6)-(8), actual values during this phase are mainly determined by the ratio of ΔU_r to ΔU_i through the influence of the AC line.

Phase II ($Z_{eq} \in (0.30, 0.55]$p.u.): the curve of actual values of (1) still maintains a downward trend during this phase, but compared with Phase I, the curve loses its smooth characteristic. When $Z_{eq} \in [0.35, 0.40]$p. u., the decline degree of the actual value of (1) is much greater than the decline degree for $Z_{eq} \in [0.40, 0.50]$p. u., and the actual value of (1) when $Z_{eq} = 0.50$ p.u. even drops to 0.386, which is the lowest actual value of voltage interaction under all conditions.

The variation trend of actual values of (1) is not sufficiently clear during this phase. This is attributed to the fact that, on the one hand, as Z_{eq} increases, the influence of ΔU_i gradually declines through the AC line. On the other hand, according to the analytical calculation process of *VIFC*, ΔU_i starts to manifest as a power imbalance within the DC transmission system, which further affects ΔU_r. The power balance state within the DC transmission system is influenced not only by ΔU_i but also by ΔU_{rdc}, which affects the power balance state of the rectifier depicted in Fig. 5. Consequently, the interwoven influence of ΔU_{rac} and ΔU_{rdc} is the fundamental cause of the erratic fluctuation in the actual value of (1) during this phase.

Phase III ($Z_{eq} \in (0.55, 1]$p.u.): the curve of actual values of (1) is a horizontal constant line with a slope of 0, which is 0.392. This observation indicates that ΔU_{rac} no longer influences ΔU_r, and ΔU_r is only affected by ΔU_{rdc}, so the actual values of (1) remain constant, i.e., $EVIF = VIFC$.

C. Comparison of Different Analytical Calculation Methods

Based on the analytical calculation method for voltage interaction proposed in Sections III-B and IV-C, the curves for the actual value of (1), *EVIF*, *IRF*, and *VIFA* are presented in Fig. 14 under the same operation conditions.

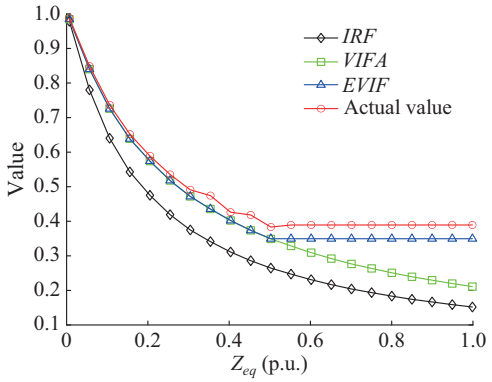

Fig. 14. Curves for actual value, *EVIF*, *IRF*, and *VIFA*.

As shown in Fig. 14, the variation trends of *EVIF*, *IRF*, and *VIFA* are consistent when $Z_{eq} \in (0, 0.50]$p.u., but the error of *IRF* and the other two indices gradually increases. Beginning at $Z_{eq} > 0.50$ p. u., the decrease rate in *IRF* and *VIFA* gradually slows, while both maintain a downward trend. At the same time, the *VIFA* begins to fall below the *EVIF*, so $Z_{eq} = 0.50$ p.u. is regarded as the "inflection point" to distinguish between different types of EDC transmission systems.

Comparing the results of *EVIF*, *IRF*, and *VIFA* with the actual value of (1), the *EVIF* is closest to the actual value of (1), especially when both indices have the same "inflection point" near $Z_{eq} = 0.50$ p.u. ("inflection point" of actual value is $Z_{eq} = 0.55$ p.u.).

The variations of error statistics err_{EVIF}, err_{VIFA}, and err_{IRF} between the analytical calculation result and the actual value of (1) under different Z_{eq} are statistically presented in Fig. 15, and Table III summarizes the maximum, minimum, average, and variance values of err_{EVIF}, err_{VIFA}, and err_{IRF}. It is evident that the err_{IRF} is significantly higher than both err_{EVIF} and err_{ac} during all phases in Fig. 15. The err_{EVIF} and err_{VIFA} gradually increase with the increase of Z_{eq} during $Z_{eq} \in (0, 0.30]$p. u.; however, these error values remain controlled within 5%. When $Z_{eq} \in (0.30, 0.55]$p.u., as analyzed in Section VI-B, irregular fluctuations in the actual value of (1) lead to erratic errors in all indices, with err_{EVIF} reaching a peak of 10.58% within this range. As Z_{eq} continues to increase, err_{EVIF} stabilizes at 10.11%. In contrast, the calculation results of *IRF* and *VIFA* still account for parameters such as Z_{eq}, Z_{sr}, P_i, Q_i, P_{ri}, Q_{ri}, resulting in a further widening of the corresponding errors within the range of $Z_{eq} \in (0.55, 1]$ p.u., and there are no trends of error reduction or stabilization.

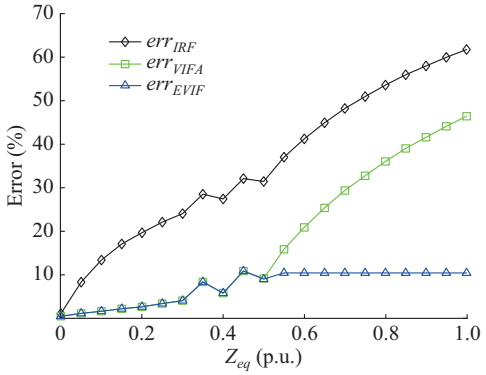

Fig. 15. Comparison of err_{EVIF}, err_{VIFA}, and err_{IRF}.

TABLE III
ERROR STATISTICS OF EACH INDEX

Error	The minimum value	The maximum value	Average value	Variance value
err_{EVIF}	0.38	10.58	7.11	2.96
err_{VIFA}	0.38	45.52	17.74	51.65
err_{IRF}	0.98	60.58	34.37	62.86

In summary, the analysis indicates that, compared with *IRF* and *VIFA*, the *EVIF* can more accurately evaluate the voltage interaction degree as measured by the physical voltage interaction ratio in (1).

VII. CONCLUSION

This paper presents an analytical calculation method for voltage interaction in the EDC transmission system, and provides a comprehensive study of the typical structure, evaluation index, analytical calculation method, type distinction, and parameter dependence of EDC transmission systems.

The main conclusions are as follows.

1) The variation characteristics of the actual value of voltage interaction are analyzed in a constructed dynamic simulation model, validating the accuracy of the analytical calculation method of the proposed *EVIF*.

2) The *EVIF* validly distinguishes between R-EDC and P-EDC transmission systems by interaction mechanisms rather than structure. In a strong AC network, when $EVIF > 0.352$, AC network interactions dominate interaction caused by the controller responses, classifying the system as P-EDC transmission system.

3) The proposed method offers high calculational efficiency without the need for simulation modeling or measurements, making it widely applicable and scalable in engineering practice.

Additionally, since the proposed method is based on reasonable assumptions regarding the control characteristics of LCC-based EDC transmission systems under small disturbance, its analytical calculation results may exhibit some deviations from actual values, and the analytical process should be refined in future research to achieve higher accuracy under small disturbance. While this method cannot be directly applied to the calculation of voltage interaction in VSC-based EDC transmission systems, it offers a valuable theoretical framework for the analysis of voltage interaction in such systems.

REFERENCES

[1] L. Zheng and S. Ma, "Damping characteristic analysis and optimization of wind-thermal-bundled power transmission by LCC-HVDC systems," *Journal of Modern Power Systems and Clean Energy*, vol. 12, no. 1, pp. 299-312, Jan. 2024

[2] M. Barnes, D. V. Hertem, S. P. Teeuwsen *et al*., "HVDC systems in smart grids," *Proceedings of the IEEE*, vol. 105, no. 11, pp. 2082-2098, Nov. 2017.

[3] D. H. Kwon, Y. J. Kim, and S. I. Moon, "Modeling and analysis of an LCC HVDC system using DC voltage control to improve transient response and short-term power transfer capability," *IEEE Transactions on Power Delivery*, vol. 33, no. 4, pp. 1922-1933, Aug. 2018.

[4] S. Henry, O. Despouys, R. Adapa *et al*., "Influence of embedded HVDC transmission on system security and AC network performance," Joint Working Group C4/B4/C1.604, Paris, France, Tech. Rep., Apr. 2013.

[5] J. Xu, T. Lan, S. Liao *et al*., "An on-line power/voltage stability index for multi-infeed HVDC systems," *Journal of Modern Power Systems and Clean Energy*, vol. 7, no. 5, pp. 1094-1104, Mar. 2019.

[6] D. H. A. Lee and G. Andersson, "An equivalent single-infeed model of multi-infeed HVDC systems for voltage and power stability analysis," *IEEE Transactions on Power Delivery*, vol. 31, no. 1, pp. 303-312, Feb. 2016.

[7] B. Rehman, C. Liu, H. Li *et al*., "Analysis on local and concurrent commutation failure of multi-infeed HVDC considering inter-converter interaction," *Journal of Modern Power Systems and Clean Energy*, vol. 10, no. 4, pp. 1050-1059, Jun. 2022.

[8] I. Fernando, K. Kent, I. Davies *et al*., "Parameters for planning and evaluation of multi-infeed HVDC schemes," CIGRE 2007 Osaka Symposium, Osaka, Japan, Tech. Rep., Sept. 2007.

[9] D. K. B. Davies, A. Williamson, A. M. Gole *et al*., "Systems with multiple DC infeed," CIGRE Publication 364 (WG B4.41), Paris, France, Tech. Rep., Aug. 2008.

[10] D. L. H. Aik and G. Andersson, "Use of participation factors in modal voltage stability analysis of multi-infeed HVDC systems," *IEEE Transactions on Power Delivery*, vol. 13, no. 1, pp. 203-211, Jan. 1998.

[11] CIGRE, "On voltage and power stability in AC/DC systems," CIGRE Brochure 222 (WG B4.05), Paris, France, Tech. Rep., Aug. 2002.

[12] P. F. de Toledo, B. Bergdahl, and G. Asplund, "Multiple infeed short circuit ratio – aspects related to multiple HVDC into one AC network," in *Proceedings of 2005 IEEE/PES Transmission & Distribution Conference & Exposition*: *Asia and Pacific*, Dalian, China, Aug. 2005, pp. 1-6.

[13] W. Lin, Y. Tang, and G. Bu, "Definition and application of short circuit ratio for multi-infeed AC/DC power systems," *Proceedings of the CSEE*, vol. 28, no. 31, pp. 1-8, Nov. 2008.

[14] D. L. H. Aik and G. Andersson, "Analysis of voltage and power interactions in multi-infeed HVDC systems," *IEEE Transactions on Power Delivery*, vol. 28, no. 2, pp. 816-824, Apr. 2013.

[15] D. L. H. Aik and G. Andersson, "Power stability analysis of multi-infeed HVDC systems," *IEEE Transactions on Power Delivery*, vol. 13, no. 3, pp. 923-931, Jul. 1998.

[16] C. Guo, P. Cui, and C. Zhao, "Optimization and configuration of control parameters to enhance small-signal stability of hybrid LCC-MMC HVDC system," *Journal of Modern Power Systems and Clean Energy*, vol. 10, no. 1, pp. 213-221, Jan. 2022

[17] H. Xiao and Y. Li, "Multi-infeed voltage interaction factor: a unified measure of inter-inverter interactions in hybrid multi-infeed HVDC systems," *IEEE Transactions on Power Delivery*, vol. 35, no. 4, pp. 2040-2048, Aug. 2020.

[18] Z. Wang, J. Huang, L. Cheng *et al*., "Planning and application of embedded DC transmission technology in the provincial transmission power grid," *Electric Power Engineering Technology*, vol. 41, no. 6, pp. 65-74, Nov. 2022.

[19] S. H. A. Niaki, Z. Chen, B. Bak-Jensen *et al*., "DC protection criteria for multi-terminal HVDC system considering transient stability of embedded AC grid," *International Journal of Electrical Power & Energy Systems*, vol. 157, p. 109815, Jun. 2024.

[20] F. R. V. de A. Pedroso, M. T. Bassini, M. A. B. Horita *et al*., "HVDC multi-infeed analysis of the Brazilian transmission system and possible mitigation methods," *CSEE Journal of Power and Energy Systems*, vol. 4, no. 4, pp. 487-494, Dec. 2018.

[21] D. Huang, Y. Shu, J. Ruan *et al*., "Ultra high voltage transmission in China: developments, current status and future prospects," *Proceedings of the IEEE*, vol. 97, no. 3, pp. 555-583, Mar. 2009.

[22] E. Pierri, O. Binder, N. G. A. Hemdan *et al*., "Challenges and opportunities for a European HVDC grid," *Renewable and Sustainable Energy Reviews*, vol. 70, pp. 427-456, Apr. 2017.

[23] X. Chen, M. Han, and C. Liu, "Impact of control modes on voltage interaction between multi-infeed AC-DC system," *Automation of Electric Power Systems*, vol. 36, no. 2, pp. 58-63, Jan. 2012.

[24] X. Guo, J. Guo, and C. Wang, "Practical calculation method for multi-infeed short circuit ratio influenced by characteristics of external characteristics of DC system," *Proceedings of the CSEE*, vol. 35, no. 9, pp. 2143-2151, May 2015.

[25] X. Chen, A. M. Gole, and M. Han, "Analysis of mixed inverter/rectifier multi-infeed HVDC systems," *IEEE Transactions on Power Delivery*, vol. 27, no. 3, pp. 1565-1573, Jul. 2012.

[26] X. Chen, M. Han, C. Liu *et al*., "System strength evaluation of multi-infeed HVDC system integrated with rectifier stations," *Proceedings of the CSEE*, vol. 32, no. 1, pp. 101-107, Jan. 2012.

[27] F. Dorfler and F. Bullo, "Kron reduction of graphs with applications to electrical networks," *IEEE Transactions on Circuits and Systems I*: *Regular Papers*, vol. 60, no. 1, pp. 150-163, Jan. 2013.

Cangbi Ding received the B.S. degree in automation from Southeast University Chengxian College, Nanjing, China, in 2019, and the M.S. degree from Nanjing University of Posts and Telecommunications, Nanjing, China, in 2022. He is currently pursuing the Ph.D. degree at the College of Automation Engineering, Nanjing University of Aeronautics and Astronautics, Nanjing, China. His main research interest includes planning and control of high-voltage direct current (HVDC) systems.

Chenyi Zheng received the B.S. degree from the South China University of Technology, Guangzhou, China, in 2015, and the Ph.D. degree from Southeast University, Nanjing, China, in 2023. He is currently a Lecturer with the College of Information Science and Technology and Artificial Intelligence, Nanjing Forestry University, Nanjing, China. His research interests include power system operation and control and HVDC power transmission.

Yi Tang received the B.S. and Ph.D. degrees from Harbin Institute of Technology, Harbin, China, in 2000 and 2006, respectively. He is currently a Professor with the School of Electrical Engineering, Southeast University, Nanjing, China. His research interests include power system operation and control, cyber-physical system, and application of artificial intelligence in pow-

er systems.

Chaohai Zhang received the B.A., M.S., and Ph.D. degrees from the Harbin Institute of Technology (HIT), Harbin, China, the P.L.A. Navy Aeronautical Engineering Academy (NAEA), Yantai, China, and Hong Kong Polytechnic University (HKPU), Hong Kong, China, in 1985, 1988, and 2002, respectively, all in electrical engineering. After some years' experiences of research working as a JSPS Research Fellow with Kumamoto University, Kumamoto, Japan and as a Research Engineer and Visiting Professor in Canada, he was also a Chief Research Scientist at State Grid Electric Power Research Institute, Wuhan, China, prior to joining Nanjing University of Aeronautics and Astronautics, Nanjing, China, as a Professor. His research interests include power system analysis, high-voltage engineering, and renewable energy and condition monitoring, diagnosis.

Xingning Han received the B.S. degree in electrical engineering from Hohai University, Nanjing, China, in 2011, and the Ph.D. degree in electrical engineering from Huazhong University of Science and Technology, Wuhan, China, in 2017. She is with Economic Research Institute, State Grid Jiangsu Electric Power Co., Ltd., Nanjing, China. Her research interests include planning and design of HVDC systems and optimization in power system planning and operation.